JACS
JOURNAL OF THE AMERICAN CHEMICAL SOCIETY
Article
pubs.acs.org/JACS

Thermochromic and Photoresponsive Cyanometalate Fe/Co Squares: Toward Control of the Electron Transfer Temperature

Yuan-Zhu Zhang,[†] Philip Ferko,[†] Diana Siretanu,[‡,§] Rodica Ababei,[‡,§,∥,∇] Nigam P. Rath,[†,⊥] Michael J. Shaw,[#] Rodolphe Clérac,*[,‡,§] Corine Mathonière,*[,∥,∇] and Stephen M. Holmes*[,†,⊥]

[†]Department of Chemistry and Biochemistry and [⊥]Center for Nanoscience, University of Missouri-St. Louis, St. Louis, Missouri 63121, United States

[‡]CNRS, CRPP, UPR 8641, F-33600 Pessac, France

[§]Univ. Bordeaux, CRPP, UPR 8641, F-33600 Pessac, France

[∥]CNRS, ICMCB, UPR 9048, F-33600 Pessac, France

[∇]Univ. Bordeaux, ICMCB, UPR 9048, F-33600 Pessac, France

[#]Department of Chemistry, University of Southern Illinois at Edwardsville, Edwardsville, Illinois 62026, United States

Supporting Information

ABSTRACT: Two structurally related and photoresponsive cyanide-bridged Fe/Co square complexes, $\{Fe_2Co_2\}$, are reported: $\{[(Tp^{Me})Fe(CN)_3]_2[Co(bpy)_2]_2[(Tp^{Me})Fe(CN)_3]_2\}\cdot 12H_2O$ (**2**) and $\{[(Tp^{Me})Fe(CN)_3]_2[Co(bpy)_2]_2[BPh_4]_2\}\cdot 6MeCN$ (**3**), where Tp^{Me} and bpy are hydridotris(3-methylpyrazol-1-yl)borate and 2,2′-bipyridine, respectively. Through electrochemical and spectroscopic studies, the Tp^{Me} ligand appears to be a moderate σ donor in comparison to others in the $[NEt_4][(Tp^R)Fe^{III}(CN)_3]$ series [where Tp^R = Tp, hydridotris(pyrazol-1-yl)borate; Tp^{Me} = hydridotris(3-methylpyrazol-1-yl)borate; pzTp = tetrakis(pyrazol-1-yl)borate; Tp* = hydridotris(3,5-dimethylpyrazol-1-yl)borate; Tp^{*Me} = hydridotris(3,4,5-trimethylpyrazol-1-yl)borate]. The spectroscopic, structural, and magnetic data of the $\{Fe_2Co_2\}$ squares indicate that thermally-induced intramolecular electron transfer reversibly converts $\{Fe^{II}_{LS}(\mu\text{-CN})Co^{III}_{LS}\}$ pairs into $\{Fe^{III}_{LS}(\mu\text{-CN})Co^{II}_{HS}\}$ units near ca. 230 and 244 K ($T_{1/2}$) for **2** and **3**, respectively (LS: low spin; HS: high spin). These experimental results show that **2** and **3** display light-induced $\{Fe^{III}_{LS}(\mu\text{-CN})Co^{II}_{HS}\}$ metastable states that relax to thermodynamic $\{Fe^{II}_{LS}(\mu\text{-CN})Co^{III}_{LS}\}$ ones at ca. 90 K. Ancillary Tp^R ligand donor strength appears to be the dominant factor for tuning electron transfer properties in these $\{Fe_2Co_2\}$ complexes.

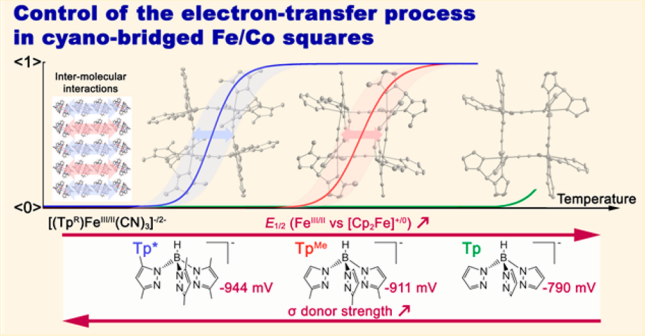

INTRODUCTION

The systematic engineering of molecular complexes with atom-economical efficiency is an exciting area of worldwide research activity, as realization of this goal may afford a diverse array of materials suitable for molecule-based high density information storage, sensor, display, and device switching applications.[1,2] Among the more celebrated switchable molecule-based materials are those derived from cyanometalates, namely those of the Prussian blue family.[3−5] These three-dimensional (3-D) coordination networks consist of an alternating array of cyanide-bridged metal ion centers to form nonstoichiometric defect solids whose overall composition, optical, and magnetic properties are strongly dependent on reagent stoichiometry, synthetic procedures, and sample history. The first photoswitchable Prussian blue analogue, $K_{0.2}Co_{1.4}[Fe(CN)_6]\cdot 6.9H_2O$, was reported by Hashimoto in 1996. In this material, spectacular changes are seen in its color and magnetism, owing to thermally- and light-induced electron transfer that reversibly interconverts diamagnetic $\{Fe^{II}_{LS}(\mu\text{-CN})Co^{III}_{LS}\}$ into paramagnetic $\{Fe^{III}_{LS}(\mu\text{-CN})Co^{II}_{HS}\}$ linkages (LS = low spin and HS = high spin).[3−5]

While many reports have described the optical, magnetic, and relaxation properties of these bistable cyanide-based Fe/Co coordination networks, the first molecular analogues were not reported until nearly a decade later. In 2004, Dunbar and coworkers reported a neutral molecular trigonal bipyramidal $\{Fe_2Co_3\}$ complex that undergoes thermally-induced changes in its magnetic and optical properties associated with intramolecular electron transfer; the behavior appears to be highly dependent on its solvation state and intermolecular environment (*vide infra*).[5b,6] In 2008, we reported that a molecular $\{Fe_4Co_4\}$ box complex could mimic both thermally- and optically-induced changes seen for three-dimensional Fe/Co Prussian blue analogues. In this cationic complex, thermal conversion of $\{Fe^{II}_{LS}(\mu\text{-CN})Co^{III}_{LS}\}$ into $\{Fe^{III}_{LS}(\mu\text{-CN})$-

Received: August 14, 2014
Published: October 23, 2014

   dx.doi.org/10.1021/ja508280n | J. Am. Chem. Soc. 2014, 136, 16854−16864

Co^{II}_{HS}} pairs reversibly occurs at ca. 252 K, and a remarkably long-lived photoinduced state is seen at lower temperatures (i.e., the relaxation time at 120 K is ca. 10 years, while those for 3-D Prussian blues range between 3 and 40 h).[4h,i,7]

Later in 2010, we reported the first example of a thermo- and photochromic $\{Fe_2Co_2\}$ square complex that exhibits an electron transfer transition temperature near ca. 177 K (Figure 1).[8] Surprisingly, the photoinduced state relaxes at a faster rate

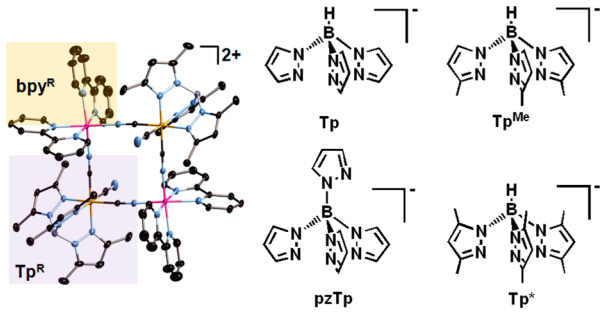

Figure 1. (left) Modular ligand substitution for tuning thermo- and photochromic behavior of $\{[(Tp^R)Fe(CN)_3]_2[Co(bpy^R)_2]\}^{2+}$ complexes. (right) Representative poly(pyrazolyl)borate ligands.

at 120 K in comparison to the octanuclear analogue (ca. 3 days versus 10 years). Subsequent work by us and also several other research groups has shown that di-,[9] tri-,[10] tetra-,[11] penta,[6] hexa-,[12] tetradecanuclear[13] complexes and 1-D coordination polymers[14] also display comparable photophysical properties, which are highly sensitive to chosen ancillary ligands *and* their solid state intermolecular environments.

Among switchable Fe/Co structural archetypes, tetranuclear analogues offer several opportunities for investigating structure−property relationships. The thermo- and photochromic squares adopt a general $\{(Tp^R)Fe(CN)_3]_2[Co(bpy^R)_2]_2[X]_2\}\cdot$ solvent stoichiometry, where Tp^R, bpy^R and X are functionalized poly(pyrazol-1-yl)borates, bidentate ligands (e.g., 2,2′-bipyridines), and charge-balancing anions, respectively (Figure 1). These molecular squares are particularly versatile platforms as they can accommodate a variety of ligands whose steric demand and donor properties may be systematically modified, thus allowing for their effects on Fe/Co square behavior to be investigated. For example, Oshio et al. briefly described the effects of ancillary ligand substitution in two structurally related $\{Fe_2Co_2\}$ squares derived from $[(Tp^R)Fe(CN)_3]^-$ anions [Tp = hydridotris(pyrazol-1-yl)borate and Tp* = hydridotris(3,5-dimethylpyrazol-1-yl)borate].[11a] In their study, three complexes were investigated as a function of Tp^R ligand substitution, where Tp^R is either Tp [hydridotris(pyrazol-1-yl)borate] or Tp* [hydridotris(3,5-dimethylpyrazol-1-yl)borate] at the iron sites, while those at the cobalt centers were limited to bpy and 4,4′-di-*tert*-butyl-2,2′bipyridine (^{tBu}bpy). In this work,[11a] electron deficient Tp square analogues remain diamagnetic up to 300 K, while electron rich Tp* derivatives display two different behaviors, depending on bpy^R ligand donor ability. With increasing temperature, a two-step electron transfer is observed at ca. 275 and 310 K for the ^{tBu}bpy analogue, while the bpy derivative remained paramagnetic between 1.8 and 300 K.[11a] Simultaneously we demonstrated that donor ligands present at the cobalt sites also play an important role in determining the electron transfer properties in $\{Fe_2Co_2\}$ complexes. Insertion of various 4,4′-disubstituted 2,2′-bipyridine ligands (bpy^R: R = H, Me) into $\{[(Tp^*)Fe(CN)_3]_2[Co(bpy^R)_2]_2\}^{2+}$ complexes changes the nature of the electron transfer regimes, transforming first-order phase transition to crossover behavior when intermolecular $\pi-\pi$ bpy interactions become weaker.[8,11b] Moreover, for the same cationic species, $\{(Tp^*)Fe(CN)_3]_2[Co(bpy)_2]_2\}^{2+}$ (bpy = 2,2′-bipyridine), a variety of anion-dependent behaviors [X = PF_6^- and $O_3SCF_3^-$] are also observed suggesting that interstitial solvent and packing arrangements also play a significant role in tuning intramolecular electron transfer properties (of reported compounds only triflate analogues display thermally- and optically-induced electron transfer).[8,11a] Further demonstrating the importance of intermolecular contacts and surroundings in these electron transfer processes, we discovered that functionalization of the bipyridyl ligands [at $Co(bpy^R)_2$ sites] with various aliphatic groups significantly alters the solubility of the molecular squares, allowing for optical and magnetic changes in both and solution states to be followed.[11b] Furthermore, we demonstrated that reversible thermal conversion of $\{Fe^{III}_{LS}(\mu\text{-}CN)Co^{II}_{HS}\}$ and $\{Fe^{II}_{LS}(\mu\text{-}CN)Co^{III}_{LS}\}$ units can be tuned in solution (by ca. 64 K between 186 and 250 K) as a function of solvent polarity, offering the prospect of solution processing.[11b]

Within these polynuclear complexes, electron transfer appears to be influenced by a variety of factors that are correlated with molecular structure and solid state packing arrangements. However, predicting which ancillary ligands will afford the correct ligand field, favorable intermolecular $\pi-\pi$ interactions, lattice solvent hydrogen bonding, and packing arrangements remains a difficult task when trying to design complexes exhibiting a preferred valence state for a chosen temperature.[5b,6−11] By analogy, this conundrum bears a striking resemblance to behaviors seen for many spin crossover complexes and understanding these structure−property issues still remains an important synthetic and intellectual challenge despite decades of extensive research activity.[15] Unfortunately, the parameters for ultimately controlling spin crossover and electron transfer are often interrelated, and determining their causal relationships remains an active arena for debate. In the case of electron transfer, Marcus−Hush theory suggests that the free energy difference and reorganization energies of the $\{Fe^{III}_{LS}(\mu\text{-}CN)Co^{II}_{HS}\}$ and $\{Fe^{II}_{LS}(\mu\text{-}CN)Co^{III}_{LS}\}$ states should be important considerations when designing polynuclear complexes that undergo intramolecular electron transfer.[16] Under the assumption that both parameters are important in establishing an energy barrier to electron transfer, we initiated a concerted research effort to understand how the redox properties of both metal sites and their environments modulate the electron transfer properties within a family of polynuclear Fe/Co complexes.

In the present contribution, we report recent efforts aimed at developing a better understanding of how metal redox potentials and their intermolecular environment modify the properties of structurally related $\{Fe_2Co_2\}$ squares. Under the assumption that σ donor strength of the Tp^R ligand selectively tunes the electron density and redox potentials of the Fe sites, it seems reasonable that the electron transfer properties of $\{Fe_2Co_2\}$ complexes would also be sensitive to these changes. We prepared a new building block, $[(Tp^{Me})Fe^{III}(CN)_3]^-$, where Tp^{Me} = hydridotris(3-methylpyrazol-1-yl)borate,[17] with the expectation that it would possess intermediate steric and electronic donor properties in comparison to those seen for Tp and Tp* analogues.[8,11,17] To further explore solid state interactions, which may also tune the temperature- and light-dependent properties, we prepared two anion-substituted

dx.doi.org/10.1021/ja508280n | J. Am. Chem. Soc. 2014, 136, 16854−16864

$\{(Tp^{Me})Fe(CN)_3\}_2[Co(bpy)_2]_2[X]_2\}$ squares. We now describe the magnetic and optical behavior of these two $\{Fe_2Co_2\}$ complexes and compare their properties to others assembled from different pyrazolylborate building blocks.[8,11]

EXPERIMENTAL SECTION

Materials. The preparation of potassium hydridotris(3-methylpyrazol-1-yl)borate $K[Tp^{Me}]$,[17] $[NEt_4]CN$,[18,19] $Co(OTf)_2$,[19] and $[NEt_4]_2[Fe_2OCl_6]$[20] are described elsewhere. $[NBu_4]PF_6$ (TCI), $CoCl_2{\cdot}6H_2O$ (Acros), $Co(ClO_4)_2{\cdot}6H_2O$ (Aldrich), 2,2′-bipyridine (Acros), Celite (Aldrich), $Na[BPh_4]$ (Acros), and deionized water were used as received. Solvents were distilled under N_2 from CaH_2 (acetonitrile) or Mg turnings (methanol). Microanalyses were performed by Robertson Microlit Laboratory. All synthetic manipulations were performed under an argon atmosphere.

Synthesis of $[NEt_4][(Tp^{Me})Fe^{III}(CN)_3]{\cdot}4.5H_2O$ (1). A MeOH (30 mL) solution of $K[Tp^{Me}]$ (1.77 g, 6.02 mmol) was slowly added to a solution of $[NEt_4]_2[Fe_2OCl_6]$ (3.02 g, 5.03 mmol) in MeCN (30 mL) over 1 h. After stirring for an additional hour, a solution of $[NEt_4]CN$ (2.81 g, 18.0 mmol) in MeCN (30 mL) was then added to afford a red mixture, which was allowed to stir for 3 h at room temperature. The red mixture was filtered through Celite and the filtrate was concentrated to dryness via rotary evaporation. The remaining brick red residue was dissolved into a 6:1 mixture (v:v) of $MeOH/H_2O$ (35 mL) and filtered again through Celite. The filtrate was concentrated under vacuum (ca. 8 mL) at 35 °C and was subsequently cooled to 0 °C for 5 min. The orange microcrystalline solid was isolated via suction filtration, washed with H_2O (3 × 5 mL) and hexane (3 × 10 mL), and dried under vacuum for 5 min at room temperature. Yield: 1.15 g (34.4%). X-ray quality crystals (**1**) were obtained via slow evaporation of a 3:1 $MeOH/H_2O$ (v:v) mixture in air. Anal. calcd for $C_{23}H_{40}BFeN_{10}O_2$ (**1**-2.5H_2O): C, 49.75; H, 7.26; N, 25.22. Found: C, 50.12; H, 7.09; N, 25.43. IR (Nujol/KBr, cm^{-1}; 300 K): 3460 (m, br), 3138 (w), 3121 (w), 2481 (m), 2121 (m), 1747 (w), 1642 (w), 1632 (w), 1504 (s), 1482 (s), 1392 (s), 1348 (s), 1198 (vs), 1173 (s), 1100 (w), 1079 (w), 1050 (vs), 1001 (m), 967 (w), 877 (w), 844 (w), 820 (w), 785 (s), 738 (s), 683 (w), 646 (w), 622 (w). UV−vis (MeCN): λ_{max}/nm ($\varepsilon_M/M^{-1}\,cm^{-1}$) 330 (1194), 415 (2815). CV (MeCN, c = 2.0 × 10^{-3} M, scan rate = 10 mV s^{-1}): E_c = −960 mV (i_c = 2.95 μA), E_a = −862 mV (i_A = 3.21 μA), $E_{1/2}$ = −911 mV.

Synthesis of $\{[(Tp^{Me})Fe(CN)_3]_2[Co(bpy)_2]_2[(Tp^{Me})Fe(CN)_3]_2\}{\cdot}12H_2O$ (2). $Co(ClO_4)_2{\cdot}6H_2O$ (37.5 mg, 0.102 mmol) and bpy (32.3 mg, 0.207 mmol) were dissolved into a 3:10 (v:v) mixture of H_2O/MeCN (13 mL) affording a yellow solution, that was allowed to stir for 30 min. Rapid addition of **1** (60.5 mg, 0.109 mmol) in MeCN (5 mL) gave a greenish-brown solution that was filtered and allowed to stand for 7 days at room temperature in air. The deposited brown needles were isolated via suction filtration, washed with MeCN (3 mL) and H_2O (5 mL), and dried under vacuum for 2 min at room temperature. Yield: 33.5 mg (49.3%). Anal. calcd for $C_{100}H_{118}B_4Co_2Fe_4N_{44}O_{11}$ (**2**-H_2O): C, 48.10; H, 4.77; N, 24.67. Found: C, 47.73; H, 4.68; N, 24.40. IR (Nujol/KBr, cm^{-1}; 300 K): 3416 (s, br), 3229 (w), 3115 (w), 3093 (w), 2505 (m), 2151 (s), 2122 (m), 2083 (w), 1641 (m), 1599 (s), 1575 (w), 1666 (m), 1503 (vs), 1491 (w), 1461 (vs), 1441 (vs), 1390 (s), 1378 (s), 1365 (m), 1345 (s), 1312 (m), 1277 (w), 1249 (w), 1196 (vs), 1153 (w), 1119 (w), 1101 (w), 1081 (w), 1051 (vs), 1022 (m), 981 (w), 967 (w), 901 (w), 888 (w), 809 (m), 801 (m), 786 (m), 770 (s), 681 (w), 651 (m), 630 (m), 621 (m), 524 (w).

Synthesis of $\{[(Tp^{Me})Fe(CN)_3]_2[Co(bpy)_2]_2[BPh_4]_2\}{\cdot}6MeCN$ (3). A mixture of $CoCl_2{\cdot}6H_2O$ (24.0 mg, 0.101 mmol), $NaBPh_4$ (68.7 mg, 0.201 mmol), and bpy (31.5 mg, 0.202 mmol) was dissolved into a 1:10 (v:v) solution of H_2O/MeCN (11 mL) at 50 °C to afford an orange mixture, that was allowed to stir for 10 h. The orange solution was added to a 15:1 (v:v) MeCN/H_2O (16 mL) solution of **1** (60.0 mg, 0.108 mmol) resulting in a brown mixture. After stirring for 2 min, the mixture was filtered and allowed to stand at 50 °C for 2 days. The brown crystals were isolated via filtration, washed with MeCN (3 mL) and H_2O (5 mL), and dried under vacuum for 2 min at room temperature. Yield: 65.0 mg (50.0%). Anal. calcd for $C_{130}H_{122}B_4Co_2Fe_2N_{32}$: C, 64.91; H, 5.12; N, 18.62. Found: C, 64.49; H, 4.84; N, 18.71. IR (Nujol, cm^{-1}; 300 K): 2497 (w), 2484 (w), 2249 (m), 2151 (s), 2125 (w), 2106 (w), 2085 (w), 2069 (w), 1599 (s), 1577 (w), 1566 (w), 1505 (m), 1491 (m), 1464 (vs), 1442 (s), 1377 (vs), 1365 (sh, s), 1346 (m), 1312 (m), 1266 (w), 1249 (w), 1197 (s), 1171 (w), 1153 (m), 1101 (w), 1078 (w), 1051 (s), 1019 (m), 918 (w), 852 (m), 812 (w), 800 (m), 766 (s), 730 (s), 705 (s) 682 (w), 651 (m), 626 (w), 615 (m), 604 (m), 536 (w).

IR and UV−vis Spectroscopies. The IR spectra were recorded as Nujol mulls between KBr plates on a Thermo-Fisher Nicolet 6700 FTIR instrument. Variable temperature data were obtained using a liquid nitrogen cooled and evacuated Janis ST-100-FTIR cryostat equipped with a Lakeshore Model 331 temperature controller. Infrared spectra of **3** collected in the presence of light were obtained via continuous white light irradiation of Nujol mulls at 79 K after 1 h from an infrared filtered Dolan-Jenner 170D Fiber-Lite light source (P = 7.1 mW cm^{-2}). Variable temperature solid state electronic spectra for **2** and **3** were obtained using Nujol mulls of samples held between KBr plates within a liquid nitrogen cooled and evacuated Graesby Specac cryostat operating between 77 and 300 K on a Varian Cary 50 Bio UV−vis spectrometer. Solution spectra for **1** were obtained as MeCN solutions on a Varian Cary Bio UV−vis spectrometer.

Electrochemistry. Electrochemistry experiments employed a three electrode system consisting of platinum disk working, Pt wire counter, and Ag/Ag^+ reference electrodes. $[NBu_4]PF_6$ (0.1 M) was used as a supporting electrolyte in MeCN solution. All potentials are reported relative to the ferrocene/ferrocenium $[Cp_2Fe/Cp_2Fe^+]$ redox couple.

Optical Reflectivity. Surface reflectivity measurements were performed on a home-built system at temperatures ranging between 10 and 300 K. A tungsten-halogen light source was used (Leica CLS 150 XD, adjustable from 0.5 to 1 W cm^{-2}) at wavelengths between 400 and 1000 nm. All measurements were calibrated against a NIST traceable reflectance standard (sphereOptics, ref SG3054). This setup collects the light reflected by the sample (that is the sum of direct and diffuse reflected light). The sample is continuously irradiated during the measurements using white spectroscopic light (P = 0.4 mW cm^{-2}). To avoid solvent loss, **2** and **3** were introduced into the sample chamber under a He atmosphere at 280 K.

Magnetic and Photomagnetic Measurements. Magnetic and photomagnetic measurements were obtained using a Quantum Design MPMS-XL SQUID magnetometer. This magnetometer operates between 1.8 and 400 K, in applied dc magnetic fields ranging from −7 to 7 T. For data collected in the absence of light, polycrystalline samples of **1**−**3** were used. Crystals of **1**−**3** were isolated via filtration from the mother liquor and left to air-dry (at 300 K) on a filter paper for <2 min. Crystalline samples of **1** (16.82 mg), **2** (19.60 mg), and **3** (28.27 mg) were placed into a sealed polyethylene bag (3 × 0.5 × 0.02 cm) and inserted into a SQUID straw. In an effort to minimize changes in magnetic properties due to desolvation, a crystalline sample of **3** (6.51 mg) was covered and thus restrained in a minimum of its frozen mother liquor within a sealed straw. No evaporation of the mother liquor was observed during the measurements. Sample mass was determined after the measurements and subsequent mother liquor evaporation. For each sample M versus H measurements were performed at 100 K to confirm the absence of ferromagnetic impurities. Magnetic data were corrected for the sample holder (plastic bag) and the diamagnetic contributions of the samples. The photomagnetic irradiation of samples was performed using a 150 W halogen/tungsten lamp (LEICA CLS 150XD) that was directed into the magnetometer cavity via an optical fiber. Finely ground crystals of **2** (3.3 mg) were packed into a preformed straw placed at 4 cm from the optical fiber. Samples of **3** (0.5 mg) were placed between two polyethylene films within a sealed straw to minimize solvent loss.

Single Crystal Crystallography. Single crystal structural data for **1** was obtained on a Nonius kappaCCD diffractometer at 120(2) K from an irregular shaped crystal using graphite collimated Mo$K\alpha$ radiation (λ = 0.71073 Å). X-ray data for **2** and **3** were collected between 79(5) and 240(2) K on a Bruker Apex-II CCD diffractometer using graphite-collimated Mo$K\alpha$ radiation. Structural data collected

dx.doi.org/10.1021/ja508280n | J. Am. Chem. Soc. 2014, 136, 16854−16864

under irradiation were performed in the presence of infrared filtered white light from a Dolan-Jenner 170D Fiber-Lite light source (P = 0.7 mW cm^{-2}). All crystals were mounted in Paratone-N oil on glass fibers. The structures were solved by direct methods (SHELXS-97)[21] and completed by difference Fourier methods (SHELXL-97).[22] Refinement was performed against F^2 by weighted full-matrix least-squares (SHELXL-2013),[22] and empirical absorption corrections (SADABS)[23] were applied. Hydrogen atoms were placed at calculated positions using suitable riding models with isotropic displacement parameters derived from their carrier atoms. Non-hydrogen atoms were refined with anisotropic displacement parameters. The structure of **1** was solved and refined in the monoclinic $P2_1/c$ space group with nine lattice water molecules. Structures of **2** and **3** were solved and refined in the triclinic (P-1) and monoclinic ($P2_1/n$) space groups and were modeled with 12 lattice water and six acetonitrile molecules, respectively. In all structures some solvents remain disordered and were refined with partial occupancies. Lattice solvents were refined with geometrical restraints (SAME, SADI, RIGU), and a displacement parameter constraint (EADP) was employed as necessary. The positions of some lattice water hydrogen atoms could not be calculated due to disorder and uncertainty in their bonding directions. Figures 1 (left) and 3–5 were generated using CrystalMaker (CrystalMaker Software Ltd., www.crystalmaker.com), while Figure 2 was created with Origin 6.1.

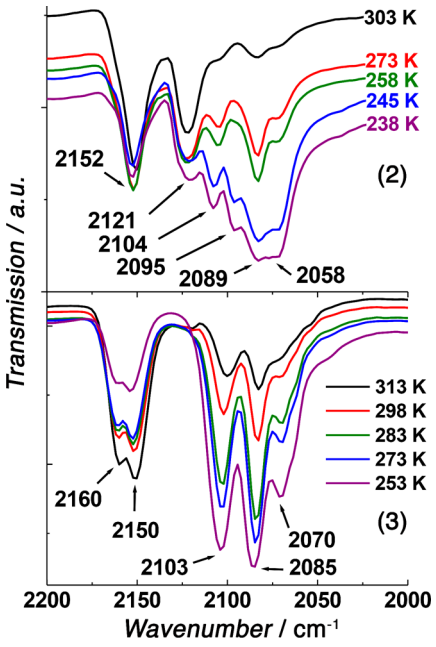

Figure 2. Variable temperature solid state infrared spectra for (top) **2** and (bottom) **3** (cooling rate of 2 K min^{-1}).

RESULTS AND DISCUSSION

Syntheses and Spectroscopic Characterization. A new tricyanoferrate complex may be prepared in moderate yield via the sequential treatment of $[NEt_4]_2[Fe_2OCl_6]$ with potassium hydridotris(3-methylpyrazol-1-yl)borate (KTp^{Me}), followed by $[NEt_4]CN$ addition. Crystalline samples are readily obtained from 6:1 (v:v) mixtures of MeOH/H_2O yielding $[NEt_4][(Tp^{Me})Fe^{III}(CN)_3]\cdot 4.5H_2O$ (**1**) as orange crystals.[24] The infrared spectrum of **1** exhibits high energy $\overline{\nu}_{BH}$ (2481 cm^{-1}) and $\overline{\nu}_{CN}$ (2121 cm^{-1}) stretches that signal the presence of low spin Fe^{III} centers.[7,25−27]

Within the structurally related family of $[NEt_4][(Tp^R)Fe^{III}(CN)_3]$ complexes, the spectroscopic and electrochemical properties may be systematically tuned over a wide range of energies and potentials in direct relation to the Tp^R ligand identity. For example, the infrared spectra display shifts in cyanide and borohydride stretching absorption energies over ca. 4 and 41 cm^{-1}, respectively, along the series indicating that significant electronic changes are induced upon Tp^R substitution (Figure S1).[24] Likewise the electronic spectra also show ligand-dependent changes in their charge-transfer bands ($Tp^R \rightarrow Fe$; LMCT), changing from ca. 409 to 445 nm, for the Tp and Tp^{*Me} derivatives, respectively. In comparison, **1** exhibits an intense absorption at ca. 415 nm, indicating that Tp^{Me} is a moderate σ donor in comparison to others in the $[NEt_4][(Tp^R)Fe^{III}(CN)_3]$ family (Figures S1 and S2).[17] Further evidence for this assumption may also be found in cyclic voltammetry data obtained for the tricyanometalate complexes (Figure S1). The data show that the $[(Tp^R)Fe(CN)_3]^{2-/-}$ redox couple can be shifted by nearly ca. 0.3 V via judicious choice of pyrazolylborate ligand, verifying that the Tp^R ligand plays a crucial role in tuning the electronic properties of the complexes. For **1**, a reversible wave ($E_{1/2}$ = −911 mV vs Fc^+/Fc) is found, which falls in between those found for electron rich $[(Tp^*)Fe(CN)_3]^{2-/-}$ (−944 mV)[25] and electron poor $[(Tp)Fe(CN)_3]^{2-/-}$ and $[(pzTp)Fe(CN)_3]^{2-/-}$ (−790 and −758 mV)[7,24,26] complexes. In comparison, both $[NEt_4]_3[Fe(CN)_6]$[27] and $[NEt_4][(Tp^{*Me})Fe(CN)_3]$[28] have more negative $Fe^{II/III}$ redox couples ($E_{1/2}$ = −1230 and −1060 mV), further demonstrating that **1** is an electron deficient complex (Figures S2 and S3). Collectively these data suggest that selective installation of functional groups onto the Tp^R ligand scaffold systematically modifies the charge density at the iron center and affords a highly tunable series of structurally related building blocks (Figures S1–S3).[17]

Subsequent treatment of **1** with cobalt(II) perchlorate hexahydrate followed by 2,2′-bipyridine in wet acetonitrile affords $\{[(Tp^{Me})Fe(CN)_3]_2[Co(bpy)_2]_2[(Tp^{Me})Fe(CN)_3]_2\}\cdot 12H_2O$ (**2**), while in the presence of sodium tetraphenylborate gives $\{[(Tp^{Me})Fe(CN)_3]_2[Co(bpy)_2]_2[BPh_4]_2\}\cdot 6MeCN$ (**3**) as an anion substituted analogue. Nujol mull infrared spectra obtained for **2** and **3** display temperature-dependent behavior that is reminiscent of several optically- and thermally-responsive cyanide-bridged Fe/Co complexes (Figures 2 and S4–S6).[5b,6−14] At 298 K, the infrared spectrum of **2** exhibits pairs of $\overline{\nu}_{BH}$ [2507 and 2488 cm^{-1}] and $\overline{\nu}_{CN}$ [2152 and 2121 cm^{-1}] stretches, with the latter being characteristic of bridging [e.g., $\{Fe^{III}_{LS}(\mu\text{-CN})Co^{II}_{HS}\}$ units] and terminal cyanides, respectively. As the temperature is lowered from 303 to 238 K, the high energy $\overline{\nu}_{CN}$ (2152 cm^{-1}) absorption decreases slightly in intensity, while new lower energy absorptions (2104, 2095, 2089, and 2058 cm^{-1}) appear to grow (Figures 2 and S4). These new $\overline{\nu}_{CN}$ stretches are typical of those belonging to bridging $[Fe^{II}_{LS}(\mu\text{-CN})Co^{III}_{LS}]$ and terminal Fe^{II}_{LS}-CN units.[7,8]

Likewise, the infrared spectrum of **3** at 298 K also displays strong $\overline{\nu}_{BH}$ [2500 and 2483 cm^{-1}] and $\overline{\nu}_{CN}$ absorptions [2160 and 2150 cm^{-1}] in addition to several weak intensity ones [2103, 2085, and 2070 cm^{-1}] (Figures 2 and S5); additional cyanide stretches attributed to lattice acetonitrile [2290 and 2250 cm^{-1}] are also present. With decreasing temperature, the low energy $\overline{\nu}_{CN}$ stretches in **3** [2103, 2085, 2070 cm^{-1}] appear to grow in intensity at the expense of the higher energy absorptions [2160 and 2150 cm^{-1}], while those belonging to acetonitrile remain unchanged. Upon warming to room temperature, the infrared spectra of **2** and **3** both return to their initial appearances, suggesting that thermal conversion of $\{Fe^{III}_{LS}(\mu\text{-CN})Co^{II}_{HS}\}$ units into $\{Fe^{II}_{LS}(\mu\text{-CN})Co^{III}_{LS}\}$ ones

dx.doi.org/10.1021/ja508280n | J. Am. Chem. Soc. 2014, 136, 16854−16864

reversibly occurs via intramolecular electron transfer (Figures 2 and S5).

Infrared spectroscopy performed in the presence of white light illumination shows that electronic changes may also be optically induced (Figure S6). For slowly cooled samples of **3**, the infrared spectra at 118 and 79 K are nearly identical and display low energy $\overline{\nu}_{CN}$ stretching absorptions consistent with the presence of $\{Fe^{II}_{LS}(\mu\text{-}CN)Co^{III}_{LS}\}$ pairs [2149, 2103, 2085, and 2070 cm^{-1}]. Upon white light irradiation (1 h at 79 K; P = 7.1 mW cm^{-2}), the intensities of these low energy $\overline{\nu}_{CN}$ stretches decrease while new ones [2170 and 2160 cm^{-1}] appear at higher energies, indicating that some of the $\{Fe^{II}_{LS}(\mu\text{-}CN)Co^{III}_{LS}\}$ linkages are photochemically transformed into $\{Fe^{III}_{LS}(\mu\text{-}CN)Co^{II}_{HS}\}$ ones (Figure S6); it is worth noting that the energies and intensities of the $\overline{\nu}_{CN}$ stretches belonging to lattice acetonitrile remain unchanged. This behavior is fully consistent with partial photoinduced conversion of $Fe^{II}_{LS}/Co^{III}_{LS}$ into $Fe^{III}_{LS}/Co^{II}_{HS}$ pairs (Figure S6).

The electrochemical properties of the molecular $\{Fe_2Co_2\}$ squares were also investigated in an effort to compare their redox properties with previously reported analogues.[11a] In our hands, electrochemical data obtained for freshly prepared MeCN solutions of $\{[(Tp^*)Fe(CN)_3]_2[Co(bpy)_2]_2[X]_2\}$, where X = PF_6^- and $CF_3SO_3^-$,[8,11a] consistently displayed behavior that was nearly identical to that seen for **2** and **3**. Only after prolonged standing of these solutions, repeated electrochemical cycling, or use of wet acetonitrile (or supporting electrolyte), a complicated series of redox waves appear, suggesting that the complexes are indeed fragile in organic media. Unfortunately, under a broad range of experimental conditions using a variety of solvents, it was impossible to observe convincing electrochemical evidence that either **2** or **3** undergo reversible redox waves representative of well-defined $\{Fe_2Co_2\}$ complexes at room temperature.

Crystallographic Studies. Complex **1** crystallizes in the monoclinic $P2_1/c$ space group as orange crystals (Table S1).[24] The $[(Tp^{Me})Fe^{III}(CN)_3]^-$ anion contains a facially coordinate and tridentate hydridotris(3-methylpyrazol-1-yl)borate (Tp^{Me}) ligand and three mutually *cis*- terminal cyanides that lead to a C_{3v}-symmetric *fac*-FeN_3C_3 coordination environment (Figures 3 and S7). The sterically demanding tridentate Tp^{Me} ligand

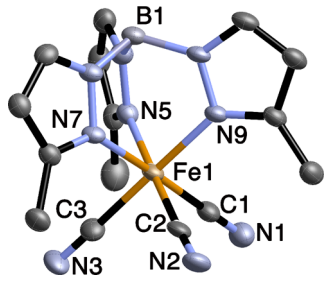

Figure 3. X-ray structure of $[(Tp^{Me})Fe^{III}(CN)_3]^-$ anion in **1** at 293 K. Lattice solvent, hydrogen atoms, and anions are eliminated for clarity, and thermal ellipsoids are at the 50% level. Fe, N, C, and B atoms are indicated in yellow, light blue, black, and gray, respectively.

distorts the coordination sphere of the anion from ideal octahedral geometry and average Fe−C and Fe−N distances of 1.924(3) and 2.004(2) Å and C−Fe−C and N−Fe−N angles of ca. 87.9(1) and 89.5(1)° are found, respectively (at 120 K; Table S2).

Compounds **2** and **3** crystallize in the triclinic (P-1) and monoclinic ($P2_1/n$) space groups, respectively (Table 1). In both structures, cyanide-bridged $[(Tp^{Me})Fe(CN)_3]^-$ and *cis*-$[Co(bpy)_2]^{2+}$ units (in a 2:2 ratio) reside in alternate corners of a molecular square. A third terminal cyanide remains per Fe site, and both adopt an *anti* orientation relative to the nearly planar $\{Fe_2(\mu\text{-}CN)_4Co_2\}$ core (Figures 4, 5, and S8−S10). Structures of **2** and **3** contain cationic $\{[(Tp^{Me})Fe(CN)_3]_2[Co(bpy)_2]_2\}^{2+}$ squares that are charge balanced by either two $[(Tp^{Me})Fe^{III}(CN)_3]^-$ or $[BPh_4]^-$ anions, respectively. In **2**, the metal ions are related via an inversion center (Figures 4 and S8), while those in **3** are crystallographically independent (Figures 5, S9 and S10). It is worth mentioning that interstitial lattice water (12) and acetonitrile (6) are also found in structures of **2** and **3**, respectively.

In **2** and **3**, the average Co−N, Fe−C, and Fe−N distances within the cationic $\{Fe_2Co_2\}$ cores exhibit significant changes as a function of temperature, particularly at the Co sites. For example, at 240 K the Co−N distances in **2** range between 1.998(4) and 2.077(4) Å [Co1−N2A and Co1−N20], while those at 100 K are smaller [1.918(4) Å, Co−N2A; 1.978(3) Å, Co−N21] falling into the typical range expected for Co^{III}_{LS} ions. Upon further inspection the average Fe−N [2.018(4) and 2.020(4) Å] and Fe−C [1.919(5) and 1.908(5) Å] distances also change slightly (Table 2) when comparing the 240 and 100 K data. Likewise, the Co−N, Fe−C, and Fe−N bond lengths in **3** also exhibit temperature-dependent changes (Table 2). At 100 K, the Co−N bonds range between 1.963(5) and 2.021(5) Å and are significantly different than those seen at 240 K [2.078(4) and 2.148(4) Å]; the Fe−C and Fe−N bonds are also slightly different at 240 and 79 K (Table 2).

Interestingly despite identical $\{Fe_2Co_2\}$ cores, both **2** and **3** exhibit noticeably different optical properties as a function of temperature. Consistent with changes seen in their infrared spectra (*vide supra*), both **2** and **3** exhibit apparent colors that are strongly dependent on sample temperature. At high temperatures (240 K) compounds **2** and **3** are brown, while at lower ones both adopt a green appearance at 100 and 79 K, respectively. Based on these observations and previous reports for structurally related complexes[8,11] it can be concluded that thermally-induced electron transfer readily converts $\{Fe^{II}_{LS}(\mu\text{-}CN)Co^{III}_{LS}\}$ into $\{Fe^{III}_{LS}(\mu\text{-}CN)Co^{II}_{HS}\}$ units in both **2** and **3**. Unlike previous reports, the average Co−N distances for **2** and **3** (Table 2)[8,11] at 240 K are only slightly longer than those seen at lower temperatures, suggesting that at this temperature, the Fe/Co pairs are in an intermediate equilibrium state, where both $\{Fe^{III}_{LS}/Co^{II}_{HS}\}$ and $\{Fe^{II}_{LS}/Co^{III}_{LS}\}$ species are present. It is also interesting to note that the charge-balancing $[(Tp^{Me})Fe^{III}(CN)_3]^-$ anions do not exhibit appreciable changes (ca. 0.01 Å) in their average Fe−C and Fe−N distances over the measured temperature range, indicating that, as expected, they do not participate in electron transfer (Table 2).

In both compounds, short intermolecular π−π interactions are found along the crystallographic *a*-direction between coordinated bpy ligands [ca. 3.428(1) Å at 100 K] in **2** (Figures 4 and S11)[28] and the bpy and tetraphenylborate anion rings [ca. 3.25(1) Å avg.] in **3** (Figures 5 and S12). In **2**, the $[(Tp^{Me})Fe^{III}(CN)_3]^-$ anions also engage in hydrogen bonds with lattice water molecules and π−π interactions along the *a*-direction (Figure S13). Completing the structure of **2**, additional hydrogen bonding also links the terminal cyanides of each $\{Fe_2Co_2\}^{2+}$ fragment to lattice water and $[(Tp^{Me})Fe^{III}(CN)_3]^-$ anions within the *bc* plane (Figures S13 and S14).

dx.doi.org/10.1021/ja508280n | J. Am. Chem. Soc. 2014, 136, 16854−16864

Table 1. Crystallographic Data for $\{[(Tp^{Me})Fe(CN)_3]_2[Co(bpy)_2]_2[(Tp^{Me})Fe(CN)_3]_2\}\cdot 12H_2O$ (2) and $\{[(Tp^{Me})Fe(CN)_3]_2[Co(bpy)_2]_2[BPh_4]_2\}\cdot 6MeCN$ (3)

compounds	2		3			
temperature, K	240(2)	100(2)	240(2)	100(2)	79(5)	79(5) (after white light irradiation)
crystal color	brown	green	brown	green	green	brown
formula	$C_{100}H_{120}B_4Co_2Fe_4N_{44}O_{12}$		$C_{130}H_{122}B_4Co_2Fe_2N_{32}$			
crystal system	triclinic		monoclinic			
space group	*P*-1		$P2_1/n$			
wavelength, Å	0.71073		0.71073			
a, Å	13.347(2)	13.214(1)	15.5769(7)	15.2959(7)	15.2955(9)	15.344(2)
b, Å	14.903(3)	14.739(2)	27.008(1)	26.677(1)	26.638(2)	26.718(3)
c, Å	16.519(3)	16.337(2)	30.954(1)	30.602(1)	30.60(2)	30.650(4)
α, °	86.703(9)	86.606(3)	90	90	90	90
β, °	67.965(9)	67.817(2)	94.781(2)	94.561(1)	94.725(3)	94.612(5)
γ, °	76.03(1)	75.689(2)	90	90	90	90
V, Å^3	2953.9(9)	2852.7(5)	12977(1)	12447.6(9)	12427(1)	12524(3)
D_c, g cm^{-3}	1.414	1.464	1.231	1.284	1.284	1.270
Z	1		4			
μ, mm^{-1}	0.829	0.858	0.531	0.554	0.555	0.5430
$R_1{}^a$	0.0583	0.0535	0.0636	0.0781	0.0975	0.0943
$wR_2{}^a$	0.1433	0.1388	0.1629	0.1874	0.2293	0.2427

$^a I \geq 2\sigma(I)$: $R_1 = \sum||F_o| - |F_c||/\sum|F_o|$, $wR_2 = \{\sum[w(F_o^2 - F_c^2)^2]/\sum[w(F_o^2)^2]\}^{1/2}$.

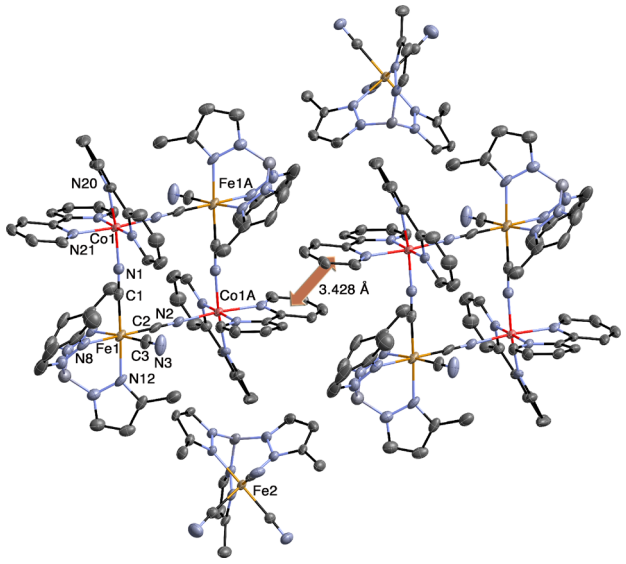

Figure 4. X-ray structure of $\{[(Tp^{Me})Fe(CN)_3]_2[Co(bpy)_2]_2\}^{2+}$ squares and $[(Tp^{Me})Fe^{III}(CN)_3]^-$ anions present in **2** at 100 K. Lattice solvent and hydrogen atoms are eliminated for clarity, and thermal ellipsoids are at the 50% level. Fe, Co, N, C, and B atoms are indicated in orange, red, light blue, black and light gray, respectively.

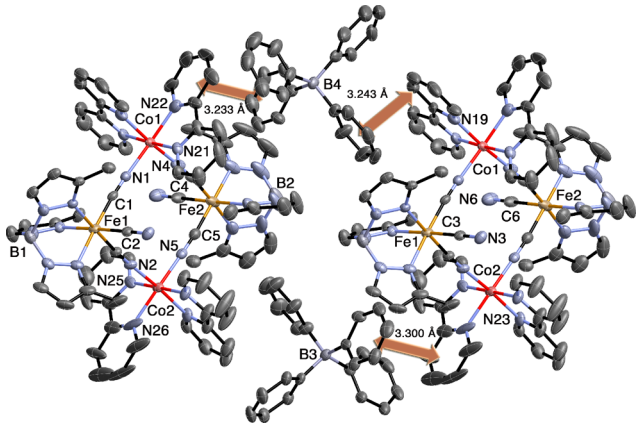

Figure 5. X-ray structure of $\{[(Tp^{Me})Fe(CN)_3]_2[Co(bpy)_2]_2\}^{2+}$ squares and $[BPh_4]^-$ anions present in **3** at 100 K. Hydrogen atoms and lattice solvent are eliminated for clarity, and thermal ellipsoids are at the 50% level. Fe, Co, N, C, and B atoms are indicated in orange, red, light blue, black and light gray, respectively.

Single-crystal X-ray diffraction studies of **3** under white light irradiation were also performed at 79 K (Figure S10), the low temperature limit of our diffractometer. In the absence of light, the cell parameters and structure of **3** are similar to those found at 100 K (Tables 1 and 2). However, under continuous light irradiation at 79 K (P = 0.7 mW cm^{-2}), the crystal color changes from green to brown after only 1 h, the metrical parameters and the average Co−N distances become comparable to those seen at 240 K. Likewise, the Fe1···Fe2 and Co1···Co2 distances significantly increase from 7.386(7) and 6.758(7) Å in the dark to 7.542(7) and 6.786(7) Å under white light irradiation at 79 K (Figure S15), while considerably longer ones [7.668(5) and 6.804(3) Å] are seen at 240 K. Consistent with the variable temperature infrared data (*vide supra*), these X-ray data strongly suggest that electron transfer can be photoinduced at 79 K, converting, at least partially, diamagnetic $\{Fe^{II}_{LS}(\mu\text{-CN})Co^{III}_{LS}\}$ units into $\{Fe^{III}_{LS}(\mu\text{-CN})\text{-}Co^{II}_{HS}\}$ pairs.

Optical Studies. Further support for this assumption may be found in solid state optical measurements collected for **2** and **3**. At room temperature, solid state reflectivity data for **2** and **3** reveal strong absorptions (i.e., low reflectivity) between 400 and 650 nm while both appear to be more reflective above 700 nm (Figure 6). These optical reflectivity spectra closely mirror the solid state UV−vis spectra for **2** and **3** (Figure S16) and the characteristics of other known thermochromic Fe/Co complexes.[8,11]

With decreasing temperatures the reflectivity signals measured above 700 nm gradually approach lower values, reaching minimum ones near ca. 200 and 150 K for **2** and **3**, respectively. At lower temperatures, the reflectivity signal intensities increase and reach maximum values at 10 K. The

dx.doi.org/10.1021/ja508280n | J. Am. Chem. Soc. 2014, 136, 16854−16864

Table 2. Selected Bond Distances (Å) and Angles (°) for $\{[(Tp^{Me})Fe(CN)_3]_2[Co(bpy)_2]_2[(Tp^{Me})Fe(CN)_3]_2\}\cdot 12H_2O$ (2) and $\{[(Tp^{Me})Fe(CN)_3]_2[Co(bpy)_2]_2[BPh_4]_2\}\cdot 6MeCN$ (3) at Different Temperatures

compounds	2		3				
temperature, K	240(2)	100(2)		240(2)	100(2)	79(5)	79(5) (after white light irradiation)
Fe1−C1	1.915(5)	1.887(5)	Fe1−C1	1.913(5)	1.890(5)	1.895(8)	1.905(8)
Fe1−C2	1.904(5)	1.890(5)	Fe1−C2	1.918(5)	1.886(5)	1.888(7)	1.905(7)
Fe1−C3	1.927(5)	1.917(5)	Fe1−C3	1.930(5)	1.908(5)	1.986(8)	1.920(8)
Co1−N1	2.015(4)	1.921(4)	Co1−N1	2.078(4)	1.973(5)	1.975(7)	2.036(7)
Co1−N2A	1.998(4)	1.918(4)	Co1−N4	2.084(4)	1.963(6)	1.977(7)	2.038(7)
Co1−N19	2.036(4)	1.957(3)	Co1−N19	2.148(4)	2.018(5)	2.008(7)	2.069(7)
Co1−N20	2.077(4)	1.977(3)	Co1−N20	2.130(5)	2.015(5)	2.024(7)	2.089(7)
Co1−N21	2.063(4)	1.978(3)	Co1−N21	2.140(4)	2.021(5)	2.019(7)	2.075(6)
Co1−N22	2.048(4)	1.960(3)	Co1−N22	2.144(4)	2.012(5)	2.014(7)	2.073(7)
Fe1···Fe1A	7.445(3)	7.208(4)	Fe2−C4	1.914(6)	1.905(7)	1.899(9)	1.913(9)
Co1···Co1A	6.847(9)	6.78(1)	Fe2−C5	1.922(5)	1.873(6)	1.868(8)	1.914(9)
Fe1−C1−N1	178.5(4)	177.4(4)	Fe2−C6	1.930(6)	1.917(6)	1.913(8)	1.929(8)
Fe1−C2−N2	174.0(4)	173.5(4)	Co2−N2	2.066(4)	1.955(5)	1.951(6)	1.996(6)
Co1−N1−C1	176.6(4)	175.1(3)	Co2−N5	2.077(4)	1.956(5)	1.964(7)	2.016(7)
Co1−N2A−C2A	170.9(4)	170.6(3)	Co2−N23	2.123(4)	2.003(5)	2.009(6)	2.070(6)
			Co2−N24	2.122(4)	2.007(5)	2.013(7)	2.070(6)
			Fe1···Fe2	7.668(5)	7.372(3)	7.386(7)	7.542(7)
			Co1···Co2	6.804(3)	6.735(4)	6.758(7)	6.786(7)
			Fe1−C1−N1	175.9(4)	175.3(4)	175.4(6)	176.9(7)
			Fe1−C2−N2	176.0(4)	175.6(4)	176.3(7)	175.2(7)
			Fe2−C4−N4	175.0(4)	174.1(5)	173.8(7)	174.2(7)
			Fe2−C5−N5	177.0(4)	175.3(5)	175.2(7)	176.0(7)
			Co1−N1−C1	172.4(4)	171.2(4)	171.6(6)	170.8(6)
			Co1−N4−C4	174.7(4)	173.7(5)	174.2(6)	174.4(6)
			Co2−N2−C2	174.7(4)	173.7(4)	173.2(6)	174.1(6)
			Co2−N5−C5	173.6(4)	172.8(4)	173.1(6)	172.9(6)

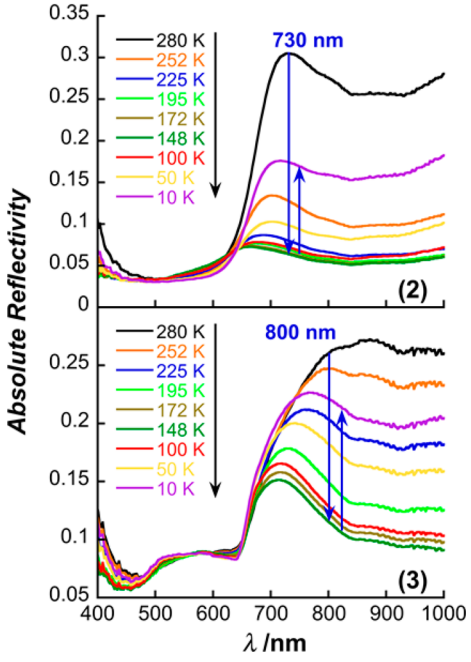

Figure 6. Temperature dependence of the optical reflectivity spectra (using white spectroscopic light, P = 0.4 mW cm^{-2}) for **2** (top) and **3** (bottom) while cooling from 280 to 10 K.

reversible nature of these optical changes is seen when samples are heated from 10 to 280 K (at the same temperature sweep rates) where superimposable spectra are obtained above ca. 130 K (Figures S17−S19).[7,8,11b]

These optical changes in **2** and **3** are better visualized by following the thermal dependence of the reflectivity data plotted at a fixed wavelength (Figures 7 and S20). With decreasing temperature, the reflectivity signal (730 nm, R_{730}) for **2** appears to rapidly decrease from 0.30 at 280 K toward a minimum value of 0.07 at 100 K (Figures 7 and S20), being consistent with behavior expected for thermally-induced electron transfer that converts $\{Fe^{III}_{LS}(\mu\text{-CN})Co^{II}_{HS}\}$ units into $\{Fe^{II}_{LS}(\mu\text{-CN})Co^{III}_{LS}\}$ pairs.[7,8,11b] At lower temperatures, R_{730} remains nearly constant down to ca. 55 K, before exhibiting a gradual increase toward 0.17 at 10 K. As the temperature is raised again, thermal hysteresis effects are seen in the reflectivity signal, reaching a maximum value of 0.26 at 51 K. Above 90 K and with a sweep rate of 4 K min^{-1}, the reflectivity values are fully recovered thus demonstrating that these thermal transformations are completely reversible (Figures 7 and S20). As previously observed in related systems,[7,8,11b] this thermal hysteresis unambiguously signals that $\{Fe^{II}_{LS}/Co^{III}_{LS}\}$ pairs are converted into $\{Fe^{III}_{LS}/Co^{II}_{HS}\}$ ones with light. For **3**, the reflectivity data collected between 280 and 10 K at 800 nm (R_{800}) globally mirror the behavior seen for **2** (Figures 7 and S20). However, with increasing temperature the thermal conversion of $\{Fe^{II}_{LS}/Co^{III}_{LS}\}$ into $\{Fe^{III}_{LS}/Co^{II}_{HS}\}$ pairs in **3** is nearly complete at 280 K, while qualitatively different behavior is found for **2**. Nevertheless, thermal hysteresis with significant reflectivity increases is observed below ca. 120 K for both complexes, with photo-initiated conversions being more efficient for **3** in comparison to **2**.

The photoresponsivity of **2** and **3** was carefully monitored at 10 K (inset of Figure 7) using incident white light of various

dx.doi.org/10.1021/ja508280n | J. Am. Chem. Soc. 2014, 136, 16854−16864

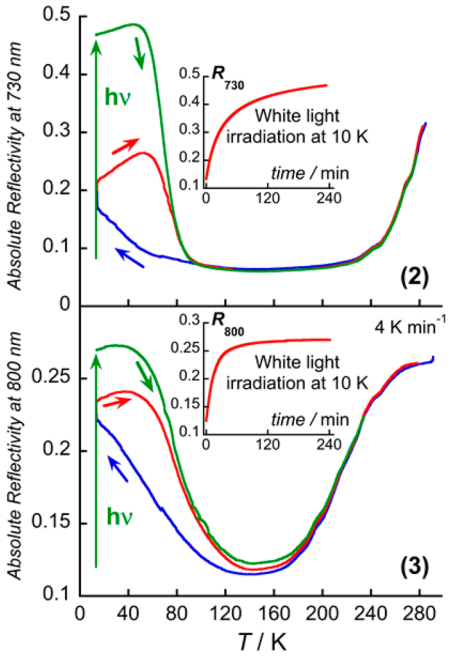

Figure 7. Temperature dependence of the optical reflectivity using white spectroscopic light (P = 0.4 mW cm^{-2}) between 280 and 10 K while cooling (blue) and heating (red); reflectivity spectra after exposure to white light (6 h; P = 0.4 mW cm^{-2}) at 10 K (green) with heating. The small blue, green, and red arrows represent the temperature sweep directions. Top: at 730 ± 5 nm (R_{730}) for **2**; inset: time evolution of R_{730} under white light irradiation (P = 0.4 mW cm^{-2}) at 10 K. Bottom: at 800 ± 5 nm (R_{800}) for **3**; inset: time evolution of R_{800} under white light irradiation (P = 0.4 mW cm^{-2}) at 10 K.

powers to establish the time and intensity necessary to photoconvert $\{Fe^{II}_{LS}(\mu\text{-CN})Co^{III}_{LS}\}$ pairs into $\{Fe^{III}_{LS}(\mu\text{-CN})Co^{II}_{HS}\}$ ones (Figures S21–S23). Surprisingly even after 6 h under 0.4 mW cm^{-2} of light exposure, complex **2** appears to only slowly reach saturation, while rapid and complete transformation of **3** occurs after ca. 1 h, confirming that **3** is highly photosensitive. After exposure to light, the reflectivity spectra of **3** collected at 10 and 280 K are remarkably similar, suggesting that identical electronic states are present (e.g., $\{Fe^{III}_{LS}/Co^{II}_{HS}\}$ pairs; Figure S23). Moreover, both **2** and **3** display comparable reflectivity spectra at 10 K after white light excitation (6 and 4 h respectively), indicating that intramolecular electron transfer occurs within the structurally and electronically similar $\{Fe_2Co_2\}$ cores (Figures 7, S22 and S23).

The thermal stability of the photoinduced $\{Fe^{III}_{LS}/Co^{II}_{HS}\}$ state in **2** and **3** was further investigated by following the decay of the reflectivity as a function of increasing temperature (at 4 K min^{-1}). Dramatic changes are observed in the optical properties at ca. 90 and 120 K for **2** and **3**, respectively (Figure 7, green curve). At these temperatures, the data indicate that the light-induced metastable $\{Fe^{III}_{LS}/Co^{II}_{HS}\}$ state is rapidly converted into the thermodynamically favored $\{Fe^{II}_{LS}/Co^{III}_{LS}\}$ form. Above ca. 200 K, the reflectivity spectra again change, adopting values that are similar to those seen at room temperature, confirming that $\{Fe^{II}_{LS}/Co^{III}_{LS}\}$ pairs are thermally converted into $\{Fe^{III}_{LS}/Co^{II}_{HS}\}$ ones above 200 K. These optical properties are entirely consistent with the light- and thermally-induced behavior seen for other bistable Fe/Co complexes.[7,8,11]

Magnetic and Photomagnetic Studies. The temperature dependence of the magnetic susceptibility, χ, has been measured on polycrystalline samples of **2** and **3** (see Experimental section; Figures 8, S24 and S25). At room

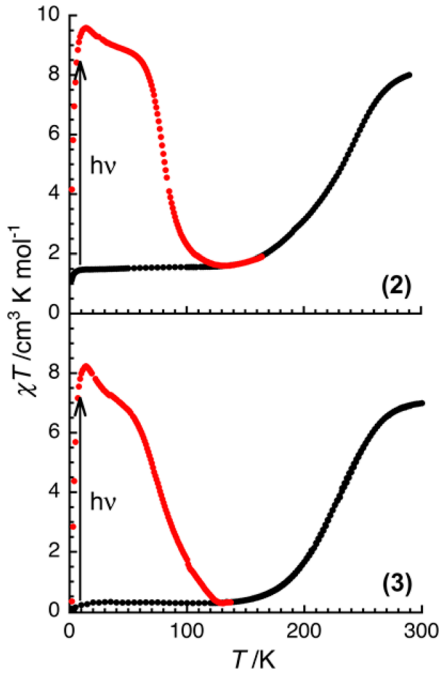

Figure 8. Temperature dependence of the χT product of (top) **2** and (bottom) **3** (with χ defined as the magnetic susceptibility equal to M/H per mole of $\{Fe_2Co_2\}$ complex) in the absence (black, 1000 Oe) and presence of light (red, 1 T) at 0.7 K min^{-1}. White light irradiation was performed at 10 K with an incident light power of P = 3 mW cm^{-2} during 15 h and 70 min for **2** and **3**, respectively.

temperature, the χT product is equal to ca. 8.0 and 7.0 cm^3 K mol^{-1} confirming the presence of 4:2 and 2:2 ratios of paramagnetic Fe^{III}_{LS} (S = $^1/_2$, $\chi T \approx 0.61$ cm^3 K mol^{-1}; Figure S26) and Co^{II}_{HS} (S = $^3/_2$, $g \approx 2.45$) centers in **2** and **3**, respectively. For both compounds, the χT products become smaller with decreasing temperatures and approach nearly constant values of 1.5 and 0.3 cm^3 K mol^{-1} at 100 K, for **2** and **3**, respectively (Figures 8, S24 and S25). Considering that **3** is a salt composed of a $\{Fe_2Co_2\}^{2+}$ square and two diamagnetic $[BPh_4]^-$ anions, the small residual χT value (0.3 cm^3 K mol^{-1})[29] seen below 120 K confirms that the tetranuclear $\{Fe_2Co_2\}^{2+}$ complexes undergo the expected paramagnetic to diamagnetic conversion with decreasing temperature. In **2**, the presence of two charge-balancing paramagnetic $[(Tp^{Me})Fe^{III}(CN)_3]^-$ (S = $^1/_2$) anions leads to a larger χT value (1.6 cm^3 K mol^{-1}) below 100 K, indicating that only the $\{Fe_2Co_2\}^{2+}$ squares participate in intramolecular electron transfer as expected.

The characteristic temperatures where a 1:1 ratio of $\{Fe^{III}_{LS}Co^{II}_{HS}\}_2$ and $\{Fe^{II}_{LS}Co^{III}_{LS}\}_2$ squares is present ($T_{1/2}$), were estimated from the maxima of the χT versus T derivative plots (i.e., $d\chi T/dT$ versus T) and are ca. 244 and 230 K for **2** and **3**, respectively (Figures S24 and S25). These values are significantly higher than found for $\{[(Tp^*)Fe(CN)_3]_2[Co(bpy)_2]_2[OTf]_2\}$ (**4**; $T_{1/2}$ = 177 K),[8] which exhibits a first-order phase transition between the low and high temperature diamagnetic and paramagnetic states, respectively. Interestingly, complexes **2** and **3** display quantitatively different behavior than

dx.doi.org/10.1021/ja508280n | J. Am. Chem. Soc. 2014, 136, 16854–16864

4, as their structural, optical, and magnetic data show no evidence for a first-order phase transition. The differential scanning calorimetry (DSC) data (Figure S27) consistently display an absence of significant enthalpic peaks between 180 and 290 K, supporting the notion that neither complex exhibits a distinct phase transition over the measured temperature range, which is reminiscent of behavior reported for $\{[(Tp^*)Fe(CN)_3]_2[Co(bpy^{Me})_2]_2[OTf]_2\}$ (**5**; $T_{1/2}$ = 174 K).[11b] Given that both **2** and **3** do display reversible optical (Figure 7) and magnetic (Figure 8) changes that are devoid of thermal hysteresis effects, we propose that thermally-induced electron transfer proceeds via a crossover between diamagnetic $\{Fe^{II}_{LS}/Co^{III}_{LS}\}$ ground and thermally accessible excited $\{Fe^{III}_{LS}/Co^{II}_{HS}\}$ states.

Since the photoactivity of **2** and **3** was clearly detected in various temperature- and light-dependent structural and spectroscopic measurements (*vide supra*, Figures 2 and 7), the magnetic properties were further investigated after light exposure at low temperatures. Remarkably, the χT product for **2** gradually approaches a maximum value of 9.4 cm^3 K mol^{-1} after 15 h of white light irradiation at 10 K (P = 3 mW cm^{-2}), while for **3**, it quickly saturates toward ca. 8.3 cm^3 K mol^{-1} after only 1 h (Figure S29). These photomagnetic data unambiguously confirm that photoinduced electron transfer occurs in both compounds, with photogeneration of paramagnetic $\{Fe^{III}_{LS}/Co^{II}_{HS}\}$ squares being more rapid for **3** in comparison to **2**, as already noted in the discussion of the optical reflectivity data (Figure S21).

To further study the relaxation behavior of the photoinduced metastable $\{Fe^{III}_{LS}/Co^{II}_{HS}\}$ state in **2** and **3**, the temperature dependence of their χT products was again measured in the absence of light. The χT values are seen to monotonically increase between 2 and ca. 14 K, reaching maximum values of 9.6 and 8.2 cm^3 K mol^{-1} for **2** and **3**, respectively (Figure 8). Between 14 and 50 K, the χT products for **2** and **3** appear to decrease without significant time decay of the magnetization (at the time scale of a single data point measurement, ca. 1 min), suggesting that ferromagnetic exchange interactions between photogenerated Fe^{III}_{LS} and Co^{II}_{HS} magnetic centers are present; we note that comparable behavior is also seen for **4**.[8] At higher temperatures, the photoinduced $\{Fe^{III}_{LS}/Co^{II}_{HS}\}$ state quickly relaxes to the thermodynamic $\{Fe^{II}_{LS}/Co^{III}_{LS}\}$ one near ca. 100 and 120 K for **2** and **3**, respectively, again confirming trends seen in the optical reflectivity data (Figure 7). Without ambiguity the structural, spectroscopic, magnetic, and photomagnetic measurements all confirm that intramolecular electron transfer may be initiated via thermal and optical means in both **2** and **3**.

CONCLUSIONS

In many thermo- and photochromic systems, a persistent question is how important are the intermolecular interactions in comparison to their intrinsic molecular characteristics. This series of $\{Fe_2Co_2\}^{2+}$ complexes (**2**, **3**, **4** and **5**) affords a unique opportunity to make these comparisons as the molecular compounds possess quasi-identical $\{Fe_2Co_2\}^{2+}$ cores but markedly different solid state intermolecular environments (Figures S11−S14).[8,11b]

First, given that the optical and magnetic data of **2** and **3** are comparable this indicates that the intrinsic energetic and electronic properties of the $\{[(Tp^{Me})Fe(CN)_3]_2[Co(bpy)_2]_2\}^{2+}$ fragment are strongly correlated. The effect of the ancillary ligands and their donor strength properties on these molecular characteristics is well illustrated when comparing the physical properties of structurally related analogues such as **2**−**5**. In **4** and **5**, significantly lower $T_{1/2}$ values (177 and 174 K)[8,11b] are found in comparison to **2** and **3** (244 and 230 K), which indicates that the diamagnetic $\{Fe^{II}_{LS}/Co^{III}_{LS}\}$ state is stabilized over a wider temperature range relative to the $\{Fe^{III}_{LS}/Co^{II}_{HS}\}$ state. It follows that within the $\{Fe(\mu\text{-}CN)Co\}$ unit, the low spin Fe^{II} state is energetically stabilized by substitution of Tp* (a good σ donor) in **4** and **5**, for Tp^{Me} (a weaker σ donor) in **2** and **3**, thus allowing for site selective tuning of the iron redox properties (Figure S1). This assumption is further supported by the fact that only structurally related analogues containing weaker donor ligands (i.e., Tp) stabilize the diamagnetic $\{Fe^{II}_{LS}/Co^{III}_{LS}\}$ form up to 300 K.[11a]

Second, the importance of solid state intercomplex contacts between the molecular squares may also be discussed on the basis of their crystal structures. In **3**, the large $[BPh_4]^-$ anions effectively isolate the square complexes (Figure S12) preventing any direct intermolecular bipyridine $\pi-\pi$ contacts, while several of these are found in structures of **2** (Figure S11). These supramolecular interactions appear to subtly modulate the electron transfer temperature observed (244 versus 230 K) for **2** and **3**, respectively, and those seen for **4** and **5** ($T_{1/2}$ = 177 versus 174 K). On the other hand, pronounced thermal hysteresis associated with a first-order phase transition is likely favored by short direct bipyridine $\pi-\pi$ interactions (3.35 Å) in the structure of **4**, while much longer contacts (3.68 Å) in **5** lead to electron transfer crossover behavior.[11b] Nevertheless, an abrupt electron transfer transition is not observed in **2** despite the fact that bipyridine $\pi-\pi$ distances are comparable to those in **4** (3.43 versus 3.35 Å).

While the appearance of a first-order phase transition is inherently related to the extent of intermolecular elastic interactions and their coupling efficiency in this system, it is overly simplistic to expect that numerous short contacts will necessarily lead to abrupt electron transfer transitions. In these $\{Fe_2Co_2\}^{2+}$ complexes, intermolecular $\pi-\pi$ bpy···bpy contacts likely provide efficient conduits for cooperative elastic interactions, with short distances favoring first-order phase transitions, but there is no obvious causal relationship linking this behavior to $T_{1/2}$ values. By comparing various structural analogues within the $\{Fe_2Co_2\}$ series, it is clear that intermolecular interactions only slightly perturb their intrinsic magnetic and optical properties.

Through various characterization techniques, we show that the optical and magnetic properties of molecular cyanide-bridged $\{Fe_2Co_2\}^{2+}$ squares can be efficiently controlled by the donor capacity of the ancillary ligand (at the iron sites) and to a lesser extent by the solid state intermolecular interactions present between the complexes. Using this approach, the associated thermo- and photochromic properties may be tuned over a wide temperature range (by ca. 60 K) where diamagnetic $\{Fe^{II}_{LS}/Co^{III}_{LS}\}$ pairs are reversibly converted into paramagnetic $\{Fe^{III}_{LS}/Co^{II}_{HS}\}$ ones. Our study highlights the role of ligand and intermolecular interactions in tunable electron transfer systems, and a better understanding of these necessary considerations may ultimately lead to the design of molecular materials that exhibit predictable and tunable electron transfer properties.

■ ASSOCIATED CONTENT

Supporting Information

Additional synthetic, electrochemical, spectroscopic, structural, reflectivity, and magnetic data. This material is available free of charge via the Internet at http://pubs.acs.org.

■ AUTHOR INFORMATION

Corresponding Authors

clerac@crpp-bordeaux.cnrs.fr
mathon@icmcb-bordeaux.cnrs.fr
holmesst@umsl.edu

Notes

The authors declare no competing financial interest.

■ ACKNOWLEDGMENTS

S.M.H. gratefully acknowledges the National Science Foundation (CHE 0914935, CAREER; CHE 0939987, X-ray upgrade; CHE 1214063), University of Missouri-St. Louis (College of Arts and Sciences Research and Undergraduate Research Awards), and Missouri Research Board for financial support. M.J.S. is grateful to the National Science Foundation for funding this work (CHE 1213680). R.C., D.S., R.A., and C.M. thank the University of Bordeaux, the ANR, the Région Aquitaine, the Institut Universitaire de France (IUF), and the CNRS for financial support. Hung Nguyen and Benjamin Quiggins are thanked for acquisition of solution infrared and UV−vis spectroscopic data. Elizabeth Hillard is also acknowledged for verifying the redox properties of $[NEt_4]_3[Fe(CN)_6]$. Mathieu Rouzières, Lionel Buisson, and Pascal Merzeau are warmly thanked for their technical help regarding the optical reflectivity setup.

■ REFERENCES

(1) (a) Sato, O.; Tao, J.; Zhang, Y.-Z. *Angew. Chem., Int. Ed.* **2007**, *46*, 2152. (b) Bleuzen, A.; Marvaud, V.; Mathonière, C.; Sieklucka, B.; Verdaguer, M. *Inorg. Chem.* **2009**, *48*, 3453.

(2) (a) Dei, A. *Angew. Chem., Int. Ed.* **2005**, *44*, 1160. (b) Simão, C.; Mas-Torrent, M.; Crivillers, N.; Lloveras, V.; Artés, J. M.; Gorostiza, P.; Veciana, J.; Rovira, C. *Nat. Chem.* **2011**, *3*, 359. (c) Prins, F.; Monrabal-Capilla, M.; Osorio, E. A.; Coronado, E.; van der Zant, H. S. J. *Adv. Mater.* **2011**, *23*, 1545.

(3) Sato, O.; Iyoda, T.; Fujishima, A.; Hashimoto, K. *Science* **1996**, *272*, 704.

(4) (a) Sato, Y.; Ohkoshi, S.-i.; Hashimoto, K. *J. Appl. Phys.* **2002**, *92*, 4834. (b) Shimamoto, N.; Ohkoshi, S.-i.; Sato, O.; Hashimoto, K. *Inorg. Chem.* **2002**, *41*, 678. (c) Sato, O.; Einaga, Y.; Iyoda, T.; Fujishima, A.; Hashimoto, K. *Inorg. Chem.* **1999**, *38*, 4405. (d) Escax, V.; Bleuzen, A.; Cartier dit Moulin, C.; Villain, F.; Goujon, A.; Varret, F.; Verdaguer, M. *J. Am. Chem. Soc.* **2001**, *123*, 12536. (e) Champion, G.; Escax, V.; Cartier dit Moulin, C.; Bleuzen, A.; Villain, F.; Baudelet, F.; Dartyge, E.; Verdaguer, M. *J. Am. Chem. Soc.* **2001**, *123*, 12544. (f) Bleuzen, A.; Lomenech, C.; Escax, V.; Villain, F.; Varret, F.; Cartier dit Moulin, C.; Verdaguer, M. *J. Am. Chem. Soc.* **2000**, *122*, 6648. (g) Cartier dit Moulin, C.; Villain, F.; Bleuzen, A.; Arrio, M.-A.; Sainctavit, P.; Lomenech, C.; Escax, V.; Baudelet, F.; Dartyge, E.; Verdaguer, M. *J. Am. Chem. Soc.* **2000**, *122*, 6653. (h) Gawali-Salunke, S.; Varret, F.; Maurin, I.; Enachescu, C.; Malarova, M.; Boukheddaden, K.; Codjovi, E.; Tokoro, H.; Ohkoshi, S.; Hashimoto, K. *J. Phys. Chem. B* **2005**, *109*, 8251. (i) Le Bris, R.; Cafun, J.-D.; Mathonière, C.; Bleuzen, A.; Létard, J. F. *New. J. Chem.* **2009**, *33*, 1255.

(5) (a) Ohkoshi, S.-i.; Tokoro, H. *Acc. Chem. Res.* **2012**, *45*, 1749. (b) Halcrow, M. A.; Dunbar, K. R.; Achim, C.; Shatruk, M. *Charge Transfer-Induced Spin-Transitions in Cyanometalate Materials*; Wiley: New York, 2013. (c) Podgajny, R.; Chorazy, S.; Nitek, W.; Rams, M.; Majcher, A. M.; Marszałek, B.; Zukrowski, J.; Kapusta, C.; Sieklucka, B. *Angew. Chem., Int. Ed.* **2013**, *52*, 896. (d) Ohkoshi, S.-i.; Hamada, Y.; Matsuda, T.; Tsunobuchi, Y.; Tokoro, H. *Chem. Mater.* **2008**, *20*, 3048. (e) Ozaki, N.; Tokoro, H.; Hamada, Y.; Namai, A.; Matsuda, T.; Kaneko, S.; Ohkoshi, S. *Adv. Funct. Mater.* **2012**, *22*, 2089. (f) Ohkoshi, S.; Imoto, K.; Tsunobuchi, Y.; Takano, S.; Tokoro, H. *Nat. Chem.* **2011**, *3*, 564.

(6) (a) Berlinguette, C. P.; Dragulescu-Andrasi, A.; Sieber, A.; Galán-Mascarós, J. R.; Güdel, H.-U.; Achim, C.; Dunbar, K. R. *J. Am. Chem. Soc.* **2004**, *126*, 6222. (b) Berlinguette, C. P.; Dragulescu-Andrasi, A.; Sieber, A.; Güdel, H.-U.; Achim, C.; Dunbar, K. R. *J. Am. Chem. Soc.* **2005**, *127*, 6766. (c) Funck, K. E.; Prosvirin, A. V.; Mathonière, C.; Clérac, R.; Dunbar, K. R. *Inorg. Chem.* **2011**, *50*, 2782.

(7) Li, D.-F.; Clérac, R.; Roubeau, O.; Harté, E.; Mathonière, C.; Le Bris, R.; Holmes, S. M. *J. Am. Chem. Soc.* **2008**, *128*, 4929.

(8) Zhang, Y.-Z.; Li, D.-F.; Clérac, R.; Kalisz, M.; Mathonière, C.; Holmes, S. M. *Angew. Chem., Int. Ed.* **2010**, *49*, 3752.

(9) Koumousi, E. S.; Jeon, I.-R.; Gao, Q.; Dechambenoit, P.; Woodruff, D. N.; Merzeau, P.; Buisson, L.; Jia, X.; Li, D.-F.; Volatron, F.; Mathonière, C.; Clérac, R. *J. Am. Chem. Soc.*, **2014**, *136*, 15461.

(10) Liu, T.; Dong, D.-P.; Kanegawa, S.; Kang, S.; Sato, O.; Shiota, Y.; Yoshizawa, K.; Hayami, S.; Wu, S.; He, C.; Duan, C.-Y. *Angew. Chem., Int. Ed.* **2012**, *51*, 4367.

(11) (a) Nihei, M.; Sekine, Y.; Suganami, N.; Nakazawa, K.; Nakao, A.; Murakami, Y.; Oshio, H. *J. Am. Chem. Soc.* **2011**, *133*, 3592. (b) Siretanu, D.; Li, D.-F.; Buisson, L.; Bassani, D. M.; Holmes, S. M.; Mathonière, C.; Clérac, R. *Chem.—Eur. J.* **2011**, *17*, 11704. (c) Mercurol, J.; Li, Y.-L.; Pardo, E.; Risset, O.; Seuleiman, M.; Rousselière, H.; Lescouëzec, R.; Julve, M. *Chem. Commun.* **2010**, *46*, 8995. (d) Mondal, A.; Li, Y.; Seuleiman, M.; Julve, M.; Toupet, L.; Buron-Le Cointe, M.; Lescouezec, R. *J. Am. Chem. Soc.* **2013**, *135*, 1653.

(12) Nihei, M.; Okamoto, Y.; Sekine, Y.; Hoshino, N.; Shiga, T.; Liu, I. P.-C.; Oshio, H. *Angew. Chem., Int. Ed.* **2012**, *51*, 6361.

(13) Mitsumoto, K.; Oshiro, E.; Nishikawa, H.; Shiga, T.; Yamamura, Y.; Saito, K.; Oshio, H. *Chem.—Eur. J.* **2011**, *17*, 9612.

(14) (a) Liu, T.; Zhang, Y.-J.; Kanegawa, S.; Sato, O. *Angew. Chem., Int. Ed.* **2010**, *49*, 8645. (b) Liu, T.; Zhang, Y.-J.; Kanegawa, S.; Sato, O. *J. Am. Chem. Soc.* **2010**, *132*, 8250. (c) Dong, D.-P.; Liu, T.; Kanegawa, S.; Kang, S.; Sato, O.; He, C.; Duan, C.-Y. *Angew. Chem., Int. Ed.* **2012**, *51*, 5119. (d) Hoshino, N.; Iijima, F.; Newton, G. N.; Yoshida, N.; Shiga, T.; Nojiri, H.; Nakao, A.; Kumai, R.; Murakai, Y.; Oshio, H. *Nat. Chem.* **2012**, *4*, 921. (e) Liu, T.; Zheng, H.; Kang, S.; Shiota, Y.; Hayami, S.; Mito, M.; Sato, O.; Yoshizawa, K.; Kanegawa, S.; Chunying, D. *Nat. Commun.* **2013**, *4*, 2826.

(15) (a) *Spin Crossover in Transition Metal Compounds* ; Gütlich, P., Goodwin, H. A., Eds.; Springer: Berlin, 2004, Vols. *I*−*III*. (b) Varret, F.; Noguès, M.; Goujon, A. In *Magnetism: Molecules to Materials*; Miller, J., Drillon, M., Eds.; Wiley: New York, 2001; Vol. 2. (c) Gütlich, P.; Garcia, Y.; Woïke, T. *Coord. Chem. Rev.* **2001**, *219*, 839. (d) Boillot, M.-L.; Roux, C.; Audière, J.-P.; Dausse, A.; Zarembovitch, J. *Inorg. Chem.* **1996**, *35*, 3975. (e) Decurtins, S.; Gütlich, P.; Kohler, C. P.; Spiering, H.; Hauser, A. *Chem. Phys. Lett.* **1984**, *105*, 1. (f) Bonhommeau, S.; Molnár, G.; Galet, A.; Zwick, A.; Real, J. A.; McGarvey, J. J.; Bousseksou, A. *Angew. Chem., Int. Ed.* **2005**, *44*, 4069. (g) Cobo, S.; Ostrovskii, D.; Bonhommeau, S.; Vendier, L.; Molnár, G.; Salmon, L.; Tanaka, K.; Bousseksou, A. *J. Am. Chem. Soc.* **2008**, *130*, 9019. (h) McGarvey, J. J.; Lawthers, J. *Chem. Commun.* **1982**, 906. (i) Bousseksou, A.; Molnár, G.; Salmon, L.; Nicolazzi, W. *Chem. Soc. Rev.* **2011**, *40*, 3313. (j) Halcrow, M. A. *Chem. Soc. Rev.* **2011**, *40*, 4119. (k) Kabir, M.; Van Villet, K. J. *Phys. Rev. B* **2012**, *85*, 054431. (l) Real, J. A.; Gaspar, A. B.; Muñoz, M. C. *Dalton Trans.* **2005**, 2062. (m) Duriska, M. B.; Neville, S. M.; Moubaraki, B.; Cashion, J. D.; Halder, G. J.; Chapman, K. W.; Balde, C.; Létard, J. F.; Murray, K. S.; Kepert, C. J.; Batten, S. R. *Angew. Chem., Int. Ed.* **2008**, *47*, 1.

(16) (a) Marcus, R. A. *Chem. Phys. Lett.* **1987**, *133*, 471. (b) Gray, H. B.; Walther, R.; Ellis, J. *Bioinorganic Chemistry*; Bertini, I., Gray, H. B., Lippard, S. J., Valentine, J. S., Eds.; University Science Books: Sausalito, CA, 1994. (c) Wall, M. H.; Basu, P.; Buranda, T.; Wicks, B. S.; Findsen, E. W.; Ondrias, M.; Enemark, J. H.; Kirk, M. L. *Inorg.*

Chem. **1997**, *36*, 5676. (d) Bleuzen, A.; Lomenech, C.; Dolbecq, A.; Villain, F.; Goujon, A.; Roubeau, O.; Nogues, M.; Varret, F.; Baudelet, F.; Dartyge, E.; Giorgetti, C.; Gallet, J. J.; Cartier dit Moulin, C.; Verdaguer, M. *Mol. Cryst. Liq. Cryst. Sci. Technol., Sect. A* **1999**, *334*, 965. (e) Nelsen, S. F.; Ismagilov, R. F.; Gentile, K. E.; Powell, D. R. *J. Am. Chem. Soc.* **1999**, *121*, 7108. (f) Goldsmith, R. H.; Sinks, L. E.; Kelley, R. F.; Betzen, L. J.; Liu, W. H.; Weiss, E. A.; Ratner, M. A.; Wasielewski, M. R. *Proc. Natl. Acad. Sci. U. S. A.* **2005**, *102*, 3540. (g) Lukas, A. S.; Bushard, P. J.; Weiss, E. A.; Wasielewski, M. R. *J. Am. Chem. Soc.* **2003**, *125*, 3921. (h) Weiss, E. A.; Ahrens, M. J.; Sinks, L. E.; Gusev, A. V.; Ratner, M. A.; Wasielewski, M. R. *J. Am. Chem. Soc.* **2004**, *126*, 5577.

(17) (a) Niedenzu, K.; Niedenzu, P. M.; Waner, K. R. *Inorg. Chem.* **1985**, *24*, 1604. (b) Trofimenko, S. *Scorpionates, The Coordination Chemistry of Polypyrazolylborate Liagnds*; Imperial College Press: London, 1999.

(18) Andreades, S.; Zahnow, E. W. *J. Am. Chem. Soc.* **1969**, *91*, 4181.

(19) Holmes, S. M. Molecule-Based Magnets Constructed from Hexacyanometalates, *Ph.D. Thesis*, University of Illinois at Urbana-Champaign, Urbana, IL, 1999.

(20) Armstrong, W. H.; Lippard, S. J. *Inorg. Chem.* **1985**, *24*, 981.

(21) Otwinowski, Z.; Minor, W. *Methods Enzymol.* **1997**, *276*, 307.

(22) (a) Sheldrick, G. M. *SHELX-97. Programs for Crystal Structure Solution and Refinement*; University of Göttingen: Göttingen, Germany, 1997. (b) Sheldrick, G. M. *Acta Crystallogr.* **2008**, *A64*, 112.

(23) Sheldrick, G. M. *SADABS. An empirical absorption correction program*; Bruker Analytical X-ray Systems: Madison, WI, 1996.

(24) See the Supporting Information.

(25) Li, D.-F.; Parkin, S.; Wang, G.; Yee, G. T.; Prosvirin, A. V.; Holmes, S. M. *Inorg. Chem.* **2005**, *44*, 4903.

(26) Li, D.; Clérac, R.; Parkin, S.; Wang, G.; Yee, G. T.; Holmes, S. M. *J. Am. Chem. Soc.* **2006**, *45*, 5251.

(27) (a) Mascharak, P. K. *Inorg. Chem.* **1986**, *25*, 245. (b) Pavlishchuk, V. V.; Addison, A. W. *Inorg. Chim. Acta* **2000**, *298*, 97.

(28) Janiak, C. *Dalton Trans.* **2000**, 3885.

(29) In **3**, it is worth noting that a small residual paramagnetic signal (0.3 cm^3 K mol^{-1}) is detected below ca. 120 K, suggesting that a small fraction of the compound does not undergo electron transfer. This behavior is quite common and is likely induced by defects, created, for example, by the loss of interstitial MeCN lattice solvent and the simultaneous formation of a desolvated phase (Figures S25 and S28). Hence, about 5% of the measured sample contains paramagnetic $\{Fe^{III}_{LS}/Co^{II}_{HS}\}$ squares, which do not participate in the electron transfer process (Figure 8). Similar behavior is consistently observed for **2** and other structurally related complexes.[7,8,11]